



## Electrical behavior of some silver-doped lanthanum-based CMR materials

Y. Kalyana Lakshmi, P. Venugopal Reddy\*

Department of Physics, Osmania University, Hyderabad 500 007, India

### ARTICLE INFO

#### Article history:

Received 26 September 2008

Available online 21 November 2008

#### PACS:

71.30.+h

74.25.Ha

75.47.Gk

75.47.Lx

#### Keywords:

Metal–insulator

Phase separation

Two-magnon scattering

Weak localization

### ABSTRACT

With a view to understand the structural, magnetic and electrical properties of  $\text{La}_{1-x}\text{Ag}_x\text{MnO}_3$  ( $x = 0.05\text{--}0.3$ ), a series of samples were prepared by polyvinyl alcohol (PVA) gel route. It has been found that both the metal–insulator and ferro- to paramagnetic transition temperatures after increasing up to the composition  $x = 0.20$ , are found to remain constant thereafter. The electrical resistivity vs. temperature plot of the sample  $x = 0.10$  is found to exhibit an insulating behavior below 36 K, while the sample,  $x = 0.20$  exhibits two peaks, and the observed behavior is explained on the basis of the phase separation model. The low-temperature ( $T < T_p$ ), electrical resistivity data were analyzed by a theoretical model,  $\rho = \rho_0 + \rho_2 T^2 + \rho_{4.5} T^{4.5}$ , indicating the importance of grain/domain boundary effects, electron–electron and two-magnon scattering processes. The low-temperature resistivity data ( $T < 50\text{ K}$ ) were fitted to an equation, which is based on the combined effect of weak localization, electron–electron and electron–phonon scattering.

© 2008 Elsevier B.V. All rights reserved.

### 1. Introduction

High-storage-density magnetic devices require materials with a large magnetoresistance (MR) near the room temperature. The discovery of doped manganites,  $\text{Ln}_{1-x}\text{A}_x\text{MnO}_3$  (Ln is a rare-earth ion, while A is the divalent or monovalent dopant ion) meets this technological demand to a large extent. For this reason, an intense effort has been made to synthesize new doped manganites and to understand the origin of the unique properties shown by these intriguing materials [1,2]. In these mixed oxides, the colossal magnetoresistance (CMR) phenomenon is accompanied by a wide range of exotic behaviors such as magnetic-ordering, metal–insulator transition, charge and orbital ordering. In addition, depending on temperature, pressure, doping material and its level, these novel materials exhibit rich-phase diagrams, including insulating, antiferromagnetic (AFM), paramagnetic and metallic ferromagnetic phases [1,2].

The CMR effect can be qualitatively understood in the frame work of the double-exchange (DE) interaction model proposed by Zener [3]. However, subsequent studies clearly indicated that the lattice distortion due to the Jahn–Teller (JT) effect is crucial in explaining the magnetic and transport behavior of the mixed valence manganites. Furthermore, the phase separation (PS) model which assumes the coexistence of ferromagnetic metallic

(FMM) and antiferromagnetic charge and orbital ordered insulating phases, has recently been proposed to explain the CMR effect.

Most studies on manganites focused on the doping of a divalent ion at the rare earth site. However, a few studies on monovalent doped manganites are available [4–6]. In fact, the substitution of monovalent ions (such as  $\text{Na}^+$ ,  $\text{K}^+$ ,  $\text{Ag}^+$ , etc.) for rare earth ions can also lead to the change of the valence of Mn ions, hence the DE interaction. Among these materials, manganite doped with silver are of great interest [7–10] due to their high sensitivity of magnetoresistance at room temperature via improving the microstructure of the surfaces, electrical and magnetic inhomogeneities on the grains. Moreover, as the high-conducting metal Ag provides conduction paths among grains, the resistivity of Ag-doped manganites can be much lower, making them useful for potential applications. On the other hand, it is well known that the preparation conditions can influence the microstructural, electromagnetic and transport properties of the samples. In view of these facts, an effort has been made to synthesize these materials by the polyvinyl alcohol (PVA) gel method. In recent years, the PVA method was used to synthesize various types of materials. For example, Das et al. [11] and Mandal and Ram [12] have synthesized PZT powder using PVA solution by the evaporation route. Generally PVA, is widely used as a binder for green shaping of ceramic materials and decomposing exothermally at low ignition temperatures ( $250^\circ\text{C}$ ), leaving behind hardly any residue [12]. This characteristic behavior together with the water-soluble nature has motivated the authors of the present investigation to prepare the samples by the PVA-gel route. In fact, carbon atoms in the PVA solution not only control

\* Corresponding author. Tel.: +91 40 27682242; fax: +91 40 27090020.  
E-mail address: [paduruvenugopalreddy@gmail.com](mailto:paduruvenugopalreddy@gmail.com) (P. Venugopal Reddy).

the growth of metal atoms, but also reduce them to nano-level. In view of this, a systematic investigation of electrical and magnetic behavior of nano-crystalline  $\text{La}_{1-x}\text{Ag}_x\text{MnO}_3$  prepared by the PVA-gel route has been undertaken and the results of such a study are presented here.

## 2. Experimental details

The polycrystalline materials with the compositional formula,  $\text{La}_{1-x}\text{Ag}_x\text{MnO}_3$  ( $x = 0-0.3$ ) were prepared by a novel chemical method with a reactive polymer matrix of PVA and sucrose. In this method, high-purity  $\text{La}_2\text{O}_3$  (99.99%),  $\text{AgNO}_3$  (99.9%) and  $\text{MnCO}_3$  (99.9%) were taken in stoichiometric ratio as starting materials. Later, they were converted into nitrates and mixed thoroughly maintaining pH at 1.0. To this, an aqueous polymer solution of PVA and sucrose are added drop by drop and upon heating yields a fluffy porous mass. On further heating the precursor mass in air, it decomposes and burns to give nano-crystalline powders. The powder after calcining at  $600^\circ\text{C}$  was pressed into pellets and finally sintered at  $950^\circ\text{C}$  in air for 3 h.

The phase purity of the samples was checked by powder X-ray diffraction (XRD) using Philips (X pert) diffractometer with  $\text{Cu K}\alpha$  radiation at room temperature. AC susceptibility ( $\chi$ ) measurements were carried out over a temperature range 100–350 K, to determine  $T_C$  values using a home-made sample holder designed on the basis of mutual inductance principle. The valence states of Mn ion and oxygen stoichiometry were determined using the redox titration technique. Finally, the electrical resistivity and magnetoresistance measurements were carried out using a superconducting magnetic system of OXFORD in applied fields of 1, 3 and 5 T over a temperature range, 10–310 K using the four-point probe method.

## 3. Results and discussion

### 3.1. Structural studies

The XRD patterns of all the samples are shown in Fig. 1(a), and it can be seen from the figure that the samples with  $x < 0.2$  have single phase with Rhombohedral perovskite structure and  $R\bar{3}c$  space group. The presence of second phase became apparent as Ag concentration increases gradually beyond  $x > 0.2$ . After analyzing the second phase it was identified as the unreacted metallic Ag, thereby indicating the limited solubility of Ag in  $\text{LaMnO}_3$  and the observation is in agreement with the reported ones [10]. Fig. 1(b) shows the experimental and calculated XRD patterns of LA-05 sample. The structural cell parameters of all the samples refined by the standard Rietveld technique are listed in Table 1. It can be seen from the table that the lattice parameters are found to increase initially up to the sample LA-15 and decreases thereafter.

The average crystallite sizes of the materials were estimated using the peak broadening technique [13] and the Scherrer's formula,  $\langle S \rangle = K\lambda/\beta \cos \theta$ , where  $\langle S \rangle$  is the average particle size in Å,  $K$  is the constant (shape factor 0.89),  $\lambda$  is the  $\text{Cu K}\alpha$  wavelength and  $\beta$  is the corrected full-width half-maxima of XRD peaks of the sample.  $\text{SiO}_2$  is used to correct the intrinsic width associated with the equipment. The crystallite sizes are found to be in the range 40–65 nm and are given in Table 1. In order to evaluate Mn values and oxygen content in the samples, idometric titrations [14] were carried out and the percentage of  $\text{Mn}^{4+}$  are also included in Table 1. No oxygen deficiency was found and probably this could be due to filling of vacancies with silver ions [7].

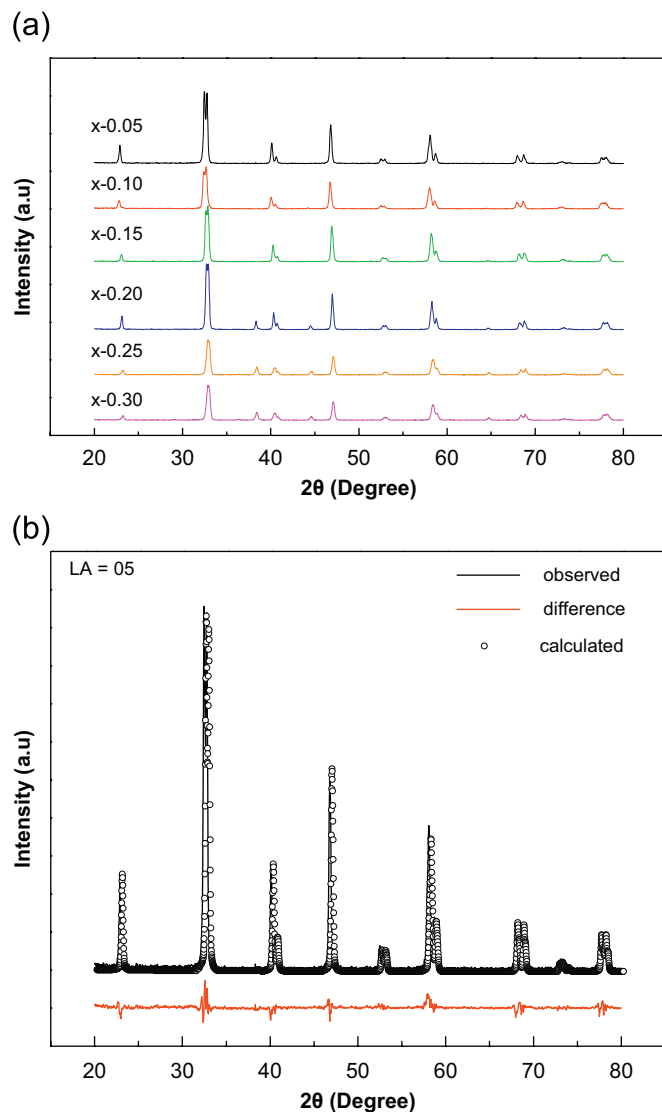


Fig. 1. (a) X-ray diffraction patterns of the Ag-doped manganites and (b) Rietveld profile fit for the X-ray diffraction pattern of LA-05 sample.

### 3.2. Magnetic transitions

The AC susceptibility ( $\chi'$ ) vs. temperature plots of Ag-doped samples are shown in Fig. 2. It can be seen from the figure that all the samples are found to exhibit a sharp ferro- to paramagnetic transition and based on the inflection point of  $d\chi'/dT$  vs.  $T$  curves,  $T_C$  values were determined (Table 2). It can be seen from the table that  $T_C$  values initially increase ( $x = 0.20$ ) and remain constant with further increase in silver doping. The observed behavior may be explained by considering the fact that doping of  $x$  Ag ions results in creating  $2x$  holes in the doping regime ( $x \leq 0.20$ ) with  $\text{Mn}^{3+}$ – $\text{Mn}^{4+}$  ratio favouring double-exchange ferromagnetism. Further, for the samples with  $x \geq 0.20$ ,  $T_C$  is constant and this may be attributed to the fact that the solubility of Ag saturates at  $x > 0.20$  forming a second phase. This in turn maintains  $\text{Mn}^{3+}/\text{Mn}^{4+}$  ratio constant thereby allowing the Curie temperature at a constant value.

### 3.3. Electrical transitions

The variation of electrical resistivity with temperature of all the samples is shown in Fig. 3 and the metal–insulator transition

**Table 1**  
Structural parameters of Ag-doped lanthanum manganites.

Sample code	Concentration of Ag	$a = b$ (Å)	$c$ (Å)	%Mn <sup>4+</sup>	$\langle S \rangle$ (nm)	Mn–O–Mn (degrees)	Mn–O (Å)
LA-05	$x = 0.05$	5.5090	13.3210	18	65	173.68	1.9448
LA-10	$x = 0.10$	5.5124	13.3217	21	45	173.69	1.9432
LA-15	$x = 0.15$	5.5131	13.3510	25	65	173.70	1.9428
LA-20	$x = 0.20$	5.5117	13.3580	30	65	173.70	1.9428
LA-25	$x = 0.25$	5.5104	13.3620	33	35	173.70	1.9428
LA-30	$x = 0.30$	5.5045	13.3520	35	40	173.70	1.9428

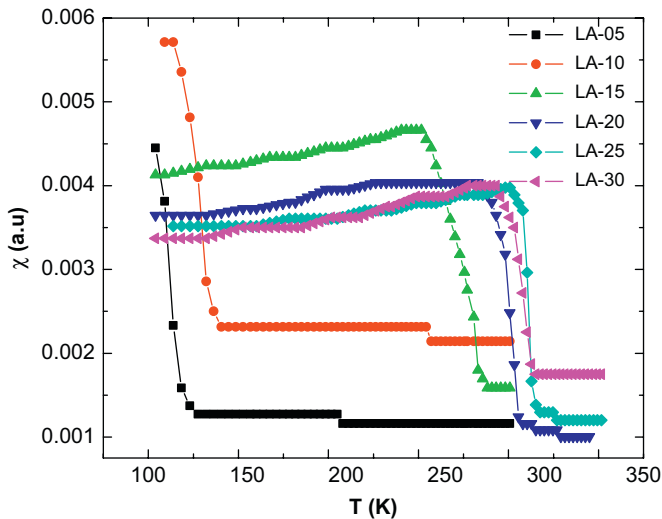


**Fig. 2.** Variation of AC susceptibility ( $\chi'$ ) with temperature for  $\text{La}_{1-x}\text{Ag}_x\text{MnO}_3$  ( $0.05 < x < 0.30$ ) manganites.

( $T_p$ ) temperatures (Table 2) are found to increase and remain constant with increasing Ag doping. It can be seen from the figure that the resistivity values of LA-05 are decreasing continuously with increasing temperature without exhibiting any change of slope within the measurement range of the present investigation. Another interesting observation is that although LA-05 is not having the metal–insulator transition ( $T_p$ ), it has surprisingly exhibited  $T_c$  at 114 K thereby indicating that the region below 114 K may be considered as ferromagnetic insulating (FMI). The observed FMI behavior cannot be explained within the framework of the double-exchange model because it predicts the coexistence of both FM as well as the metallic behavior. Therefore, the FM order at  $T < 114$  K exhibited by the sample, LA-05 might have originated from the superexchange mechanism and in fact a similar conclusion was arrived at by Yang et al. [15].

In the case of LA-10 sample, the resistivity increases with decreasing temperature reaching a maximum value at 72 K ( $T_p$ ). On further decrease of temperature,  $\rho$  decreases after reaching a minimum value at 36 K ( $T_{\min}$ ), and later on it increases once again rapidly, which is a characteristic property of an insulator [2]. In fact, a similar type of behavior was reported in the case of nonstoichiometric and Bi-doped La manganites [16,17], and low doped manganites [18–20]. Another interesting feature of this material is that under the influence of high magnetic field (5 T),  $T_{\min}$  weekend considerably (Fig. 6(a)). Another noticeable feature of the material is that its MR is not only very large but also remains almost constant over a large temperature range. Our results are in close agreement with the reports of Uehara et al. [21]. In view of this, the observed behavior may be explained by a percolative phase separation model [2,22]. According to this

model, the sample LA-10 can be considered as a mixed-phase system with intrinsic magnetic inhomogeneity as a result of the competition between AFM superexchange and FM double-exchange interaction. The FM and CO clusters coexist at low temperatures, and when the field is applied, these CO clusters will collapse, resulting in further increase of FM regions which in turn lowers the resistivity [23] thereby exhibiting large MR.

In contrast, the sample LA-15 is found to exhibit normal colossal magnetoresistance behavior with clear electrical ( $T_p$ ) and magnetic transitions ( $T_c$ ), thereby indicating that the CMR phenomenon which started emerging slowly in the case of LA-05 might have stabilized fully in the case of LA-15. Surprisingly, the sample LA-20 exhibits two transitions—one at 306 K ( $T_{p1}$ ) and the other one at 285 K ( $T_{p2}$ ) (inset of Fig. 3). As the transition at 306 K is in the vicinity of magnetic transition temperature ( $T_c$ ), it is considered as normally observed metal–insulator transition ( $T_p$ ), while the other one ( $T_{p2}$ ) observed at 285 K may be explained on the basis of the phase separation model. According to this model, for every  $\text{Ag}^{1+}$  ion substitution at  $\text{La}^{3+}$  site, two  $\text{Mn}^{3+}$  ions need to be oxidized to  $\text{Mn}^{4+}$  ions, giving rise to simultaneous occurrence of metallic  $\text{Mn}^{4+}$ -rich ferromagnetic domains in the neighborhood of Ag ions and  $\text{Mn}^{3+}$ -rich region in the neighborhood of La ions inducing phase or domain separation [24,25]. Finally, on further doping beyond  $x = 0.2$ , the Ag segregate at the grain boundaries thereby improving the conduction path between perovskite grains which in turn decreases the resistivity drastically and shifting the second peak gradually towards the high-temperature side and finally merges with the first one [8].

### 3.4. Conduction mechanism

The low-temperature resistivity data ( $T < T_p$ ) were fitted to various empirical equations, to understand the relative strengths of different scattering mechanism originating from different contributions. The experimental data of the samples ( $x \geq 0.15$ ) of the present investigation were fitted to the equation,  $\rho = \rho_0 + \rho_2 T^2 + \rho_{4.5} T^{4.5}$ , where  $\rho_0$  arises due to the grain or domain boundaries. On the other hand,  $\rho_2 T^2$  indicates the resistivity due to electron–electron scattering, while  $\rho_{4.5} T^{4.5}$  is attributed to the two-magnon scattering process. The two-magnon process is more favorable in the half-metallic band structured materials such as manganites. Fig. 4 shows the best fit for the samples,  $x \geq 0.15$ . It can be seen from the figure that all the samples are found to fit well up to  $T > 50$  K, and are found to deviate thereafter (inset of Fig. 4). Therefore, the electrical conduction below  $T < 50$  K is explained separately, in the next section.

The best fit parameters  $\rho_0$ ,  $\rho_2$  and  $\rho_{4.5}$  of all the samples are given in Table 2. It can be seen from the table that all the three parameters,  $\rho_0$ ,  $\rho_2$  and  $\rho_{4.5}$  are found to decrease with increasing dopant concentration and magnetic field and the observed behavior may be explained as follows: when the magnetic field increases, the domain enlarges reducing the value of  $\rho_0$ , while the

**Table 2**  
Experimental data of  $\text{La}_{1-x}\text{Ag}_x\text{MnO}_3$  ( $0.05 < x < 0.30$ ) materials.

Sample code	$T_p$ (K)	$T_c$ (K)	$\Delta T$ (K)	MR% at		$\rho_0$ ( $\Omega \text{ cm}$ )	$\rho_2$ ( $\Omega \text{ cm K}^{-2}$ )	$\rho_{4.5}$ ( $\Omega \text{ cm K}^{-4.5}$ )
				10 K	$T_p$			
LA-05	–	114	114	80	–	–	–	–
LA-10	72	127	55	82	91	6410.08	1.0325	$3.707 \times 10^{-6}$
LA-15	267	280	13	46	33	0.15042	$7.32 \times 10^{-6}$	$4.478 \times 10^{-13}$
LA-20	306	300	06	37	31	0.02935	$1.36 \times 10^{-6}$	$-1.91 \times 10^{-13}$
LA-25	310	308	02	36	28	0.01263	$0.54 \times 10^{-6}$	$-7.83 \times 10^{-14}$
LA-30	310	308	02	37	36	0.01544	$0.62 \times 10^{-6}$	$-7.61 \times 10^{-14}$

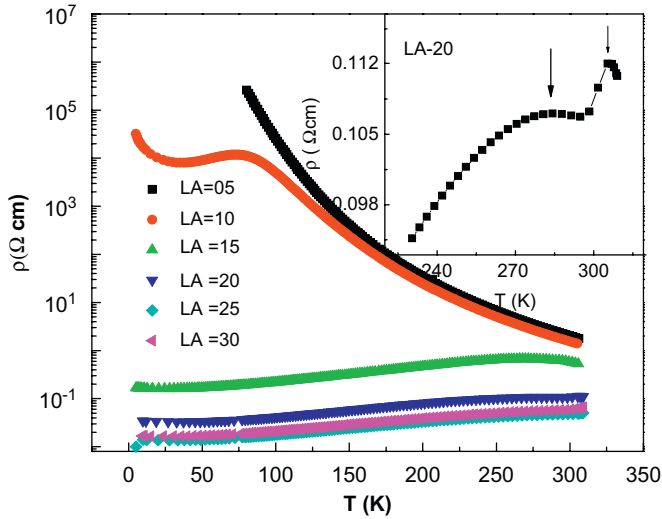


**Fig. 3.** Resistivity vs. temperature plots for different Ag concentration. Inset shows the LA-20 sample having double-peak behavior.

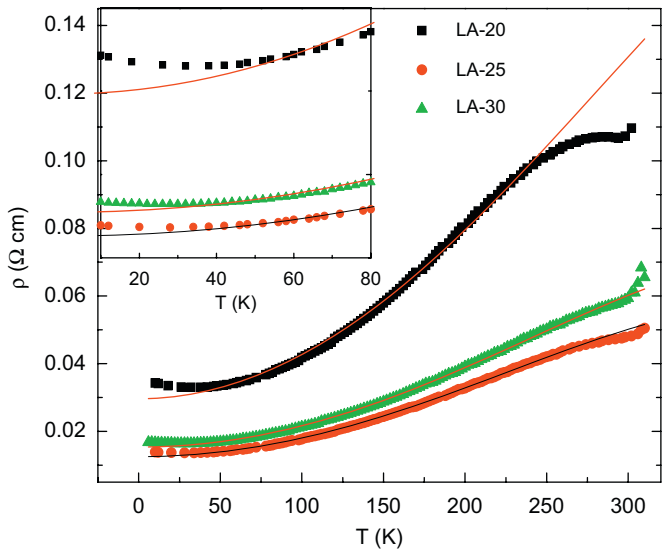


**Fig. 4.** Plots of resistivity ( $\rho$ ) vs. temperature below  $T_p$  for  $x \geq 0.20$ . The solid line gives the best fitting using the equation  $\rho = \rho_0 + \rho_2 T^2 + \rho_{4.5} T^{4.5}$ . Inset shows the deviation of the equation at low temperatures ( $T < 50$  K).

reduction in  $\rho_2$  and  $\rho_{4.5}$  could be attributed to decrease in electron spin fluctuations in the presence of magnetic field. Intrinsically, the scattering effects are suppressed from various contributions because of the parallel configuration of spins present in the domain [26].

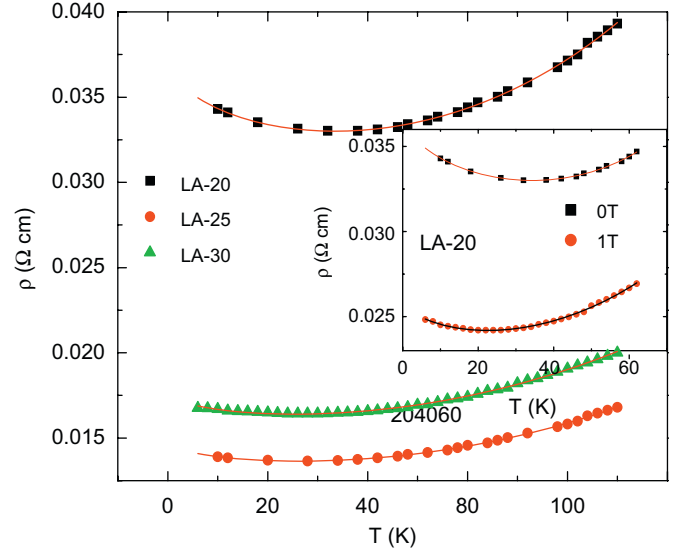


**Fig. 5.** Low-temperature electrical resistivity fitting for Ag-doped samples using the equation  $\rho(T) = \rho_0 - \rho_1 T^{1/2} + \rho_2 T^2 + \rho_5 T^5$ . Inset shows fitting data under 5 T magnetic field for LA-20 sample.

### 3.5. Low-temperature behavior

Electrical resistivity vs. temperature plots of all the samples are shown in Fig. 3. It can be seen from the figure that the first two samples exhibit insulating behavior, while the remaining ones show a slight upturn below 50 K (Fig. 5). The resistivity upturn in polycrystalline manganites is usually attributed to a different phenomenon such as Kondo effect [27], intergrain spin-polarized tunneling (ISPT) [28], enhanced electron–electron (e–e) interaction [29,30], etc. The Kondo effect is generally exhibited by a nonmagnetic system with a small percentage of magnetic impurity. As the samples under consideration have strong ferromagnetic metallic nature, possibility of Kondo effect is ruled out. According to the intergranular spin-polarized tunneling, the resistivity minimum flattens gradually with increasing field and vanishes at a critical field. In the present investigation as the resistivity minimum is still intact even in a field of 5 T, the application of the ISPT model does not arise. Therefore all the three models failed to explain the observed behavior.

However, the data is fitted using an equation which results from the combined effect of weak localization, electron–electron and electron–phonon scattering mechanism as

$$\rho(T) = \{1/(a + bT^{1/2})\} + \rho_2 T^2 + \rho_5 T^5 \quad (1)$$

where the term in parentheses arises due to the weak localization effect [29], ‘a’ is a temperature-independent residual conductivity and ‘b’ is the diffusion constant. The other two terms, namely  $\rho_2 T^2$  and  $\rho_5 T^5$ , arise due to the electron–electron and electron–phonon

**Table 3**

Low-temperature resistivity fitting ( $<50\text{ K}$ ) using equation  $\rho(T) = \rho_0 - \rho_1 T^{1/2} + \rho_2 T^2 + \rho_5 T^5$ .

Sample code	$\rho_0$ ( $\Omega\text{ cm}$ )	$\rho_1$ ( $\Omega\text{ cm K}^{-1/2}$ )	$\rho_2$ ( $\Omega\text{ cm K}^{-2}$ )	$\rho_5$ ( $\Omega\text{ cm K}^{-5}$ )
LA-05	–	–	–	–
LA-10	–	–	–	–
LA-15	0.17819	0.004120	$6.528 \times 10^{-6}$	$8.429 \times 10^{-12}$
LA-20	0.03714	0.000093	$1.061 \times 10^{-6}$	$8.399 \times 10^{-12}$
LA-25	0.0147	0.00027	$4.732 \times 10^{-6}$	$2.833 \times 10^{-12}$
LA-30	0.01732	0.00022	$3.210 \times 10^{-6}$	$1.031 \times 10^{-12}$

scattering, respectively [31]. However, we can expand Eq. (1) binomially as

$$\rho(T) = \rho_0 - \rho_1 T^{1/2} + \rho_2 T^2 + \rho_5 T^5 \quad (2)$$

where  $\rho_0 = 1/a$  and  $\rho_1 = b/a^2$  are constants.

The  $\rho(T)$  data for  $x \geq 0.15$  samples are fitted to Eq (2) (Fig. 5) and the best fit parameters are given in Table 3. It can be seen from the figure that Eq. (2) fits well both in presence and absence of magnetic field (inset of Fig. 5). In fact, Neeraj et al. [32] have also used this model to explain the low-temperature resistivity data of PBMO/Ag composites. It can be seen from Table 3 that the fitting parameters decrease with increasing doping concentration as well as magnetic field. This indicates that the weak localization, electron–electron and electron–phonon scattering decreases with Ag doping, wherein disorder decreases and the material become ordered.

### 3.6. Magnetoresistance

The percentage of magnetoresistance of all the samples has been calculated using the well-known formula

$$\text{MR}\% = \frac{\rho_{(0)} - \rho_{(H)}}{\rho_{(0)}} \times 100 \quad (3)$$

where  $\rho_{(0)}$  is the resistivity at zero magnetic field and  $\rho_{(H)}$  is the resistivity in a applied field. The  $\rho$  vs.  $T$  for LA-10 sample in the presence of 5 T field is shown in Fig. 6(a). The calculated values at low and MI transitions are given in the Table 2. Fig. 6(b) shows the MR% as a function of temperature for Ag-doped samples. It can be seen from the inset of Fig. 6(b) that, the percentage of MR is maximum at low temperatures for LA-05 samples. Surprisingly, large MR is exhibited by the sample, LA-10 over a wide temperature region below  $T_p$  (i.e. entire ferromagnetic metallic region). In contrast to the first three samples of the present investigation, MR of the samples with  $x \geq 0.15$  is found to increase almost linearly with decreasing temperature, which is a typical characteristic of a granular system. It reflects the spin-dependent electron tunneling or scattering process taking place at the grain boundaries [33], which is an extrinsic property of the granular manganites. This behavior is found to decrease with increasing Ag doping concentration, thereby indicating that the MR property of the samples slowly changes from extrinsic to intrinsic nature.

## 4. Conclusions

In conclusion, the effect of silver doping on electrical and magnetic properties is discussed. It has been found that both the metal–insulator and ferro- to paramagnetic transitions after increasing up to  $x = 0.20$ , are found to saturate thereafter. The electrical resistivity vs. temperature plot of the sample  $x = 0.10$  is found to exhibit insulating behavior below 36 K, while the sample with  $x = 0.20$  is found to exhibit two peaks, and the observed behavior is explained on the basis of phase separation. Further,

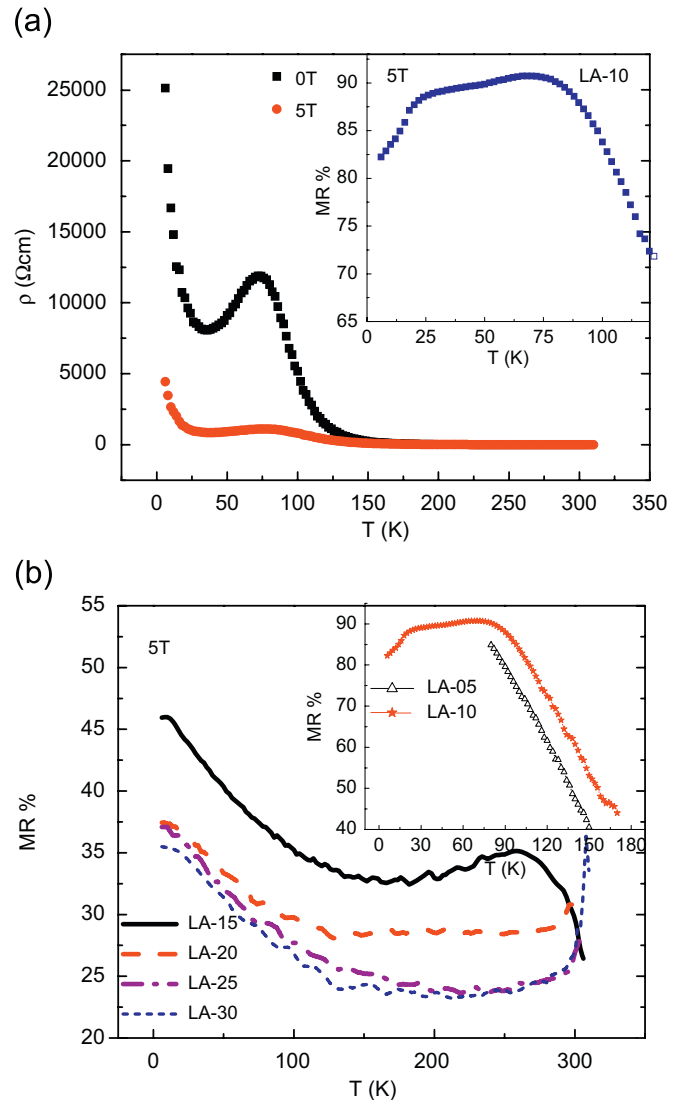


**Fig. 6.** (a) Resistivity vs. temperature for LA-10 sample in presence of 5 T field (inset shows the MR% vs. T at 5 T). (b) MR% vs. temperature plots of the Ag-doped samples for  $x \geq 0.15$ . Inset shows the MR variation for  $x = 0.05$  and  $0.10$  samples at 5 T field.

large magnetoresistance of 80% at 3 T field over a wide temperature range in the low-temperature region for  $x = 0.10$  sample is achieved. From a practical point of view, the large MR over a wide temperature range is beneficial for the application of magneto-electronics devices fabricated by the CMR materials.

## Acknowledgements

The first author is grateful to the University Grants Commission (UGC) for providing RFSMS fellowship. Authors are thankful to Dr. Rajeev Rawat, UGC-DAE Consortium for scientific Research, Indore (CSR), India, for providing MR facilities.

## References

- [1] M. D Coey, Adv. Phys. 167 (1999) 48.
- [2] E. Dogotto, T. Hotta, A. Moreo, Phys. Rep. 344 (2001) 1.
- [3] C. Zener, Phys. Rev. 82 (1951) 403.
- [4] C. Shivakumara, B. Manjunath Bellakki, S. Annigere Prakash, Y. Nagsampagi Vasanthachary, J. Am. Ceram. Soc. 90 (2007) 3852.
- [5] L.W. Lei, Z.Y. Fu, J.Y. Zhang, Mater. Lett. 60 (2007) 970.

- [6] Soma Das, T.K. Dey, *Solid State Commun.* 134 (2005) 837.
- [7] O.Yu. Gorbenko, O.V. Melnikov, A.R. Kaul, A.M. Balagurov, S.N. Bushmeleva, L.I. Koroleva, R.V. Demin, *Mater. Sci. Eng. B* 116 (2005) 64.
- [8] S.L. Ye, W.H. Song, J.M. Dai, K.Y. Wang, S.G. Wang, C.L. Zhang, J.J. Du, Y.P. Sun, J. Fang, *J. Magn. Magn. Mater.* 248 (2002) 26.
- [9] L. Pi, M. Hervieu, A. Maignan, C. Martin, B. Raveau, *Solid State Commun.* 126 (2003) 229.
- [10] M. Battabyal, T.K. Dey, *J. Phys. Chem. of Solids* 65 (2004) 1895.
- [11] R.N. Das, A. Pathak, S.K. Saha, A. Sannigrahi, P. Pramanik, *Mater. Res. Bull.* 36 (2001) 1539.
- [12] T.K. Mandal, S. Ram, *Mater. Lett.* 57 (2003) 2432.
- [13] G. Venkataiah, Y. Kalyana Lakshmi, P. Venugopal Reddy, *J. Phys. D: Appl. Phys.* 40 (2007) 721.
- [14] A.I. Vogel, *A Text Book of Quantitative Inorganic Analysis including Elementary Instrumental Analysis*, fourth ed., Longman, London, 1978.
- [15] J. Yang, W.H. Song, R.L. Zhang, Y.Q. Ma, B.C. Zhao, Z.G. Sheng, G.H. Zheng, J.M. Dai, Y.P. Sun, *Solid State Commun.* 131 (2004) 393.
- [16] V. Markovich, E. Rozenberg, G. Gorodetsky, M. Greenblatt, W.H. McCarroll, *Phys. Rev. B* 63 (2001) 054423.
- [17] Y.D. Zhao, J. Park, R.-J. Jung, H.-J. Noh, S.-J. Oh, *J. Magn. Magn. Mater.* 280 (2004) 404.
- [18] A. Dutta, N. Gayathri, R. Ranganathan, *Phys. Rev. B* 68 (2003) 054432.
- [19] Y. Moritomo, A. Asamitsu, Y. Tokura, *Phys. Rev. B* 56 (1997) 12190.
- [20] T. Tang, R.S. Huang, S.Y. Zhang, *Solid State Commun.* 147 (2008) 190.
- [21] M. Uehara, S. Mori, C.H. Chen, S.-W. Cheong, *Nature* 399 (1999) 560.
- [22] M. Mayr, A. Moreo, J.A. Verges, J. Arispe, A. Feiguin, E. Dogotto, *Phys. Rev. Lett.* 86 (2001) 135.
- [23] T. Tang, C. Tien, B.Y. Hou, *J. Alloys & Compds.* 461 (2008) 42.
- [24] G.H. Rao, J.R. Sun, J.K. Liang, *Phys. Rev. B* 55 (1997) 3742.
- [25] S.L. Ye, W.H. Song, J.M. Dai, S.G. Wang, K.Y. Wang, C.L. Yuan, Y.P. Sun, *Appl. Phys.* 88 (2000) 5915.
- [26] G. Venkataiah, P. Venugopal Reddy, *J. Magn. Magn. Mater.* 285 (2005) 343.
- [27] J. Kondo, *Prog. Theor. Phys.* 32 (1964) 37.
- [28] M. Auslender, A.E. Karkin, E. Rosenberg, G. Gorodetsky, *J. Appl. Phys.* 89 (2001) 6639.
- [29] P.A. Lee, T.V. Ramakrishnan, *Rev. Mod. Phys.* 57 (1985) 287.
- [30] B.L. Altshuler, A.G. Aronov, in: A.L. Efros, M. Pollak (Eds.), *Electron-Electron Interactions in Disordered Systems*, North-Holland, Amsterdam, 1985.
- [31] J.M. Ziman, *Electrons and Phonons*, Oxford University Press, Oxford, 1967.
- [32] P. Neeraj, D.K. Pandya, S.K. Agarwal, *J. Phys.: Condens. Matter* 19 (2007) 456224.
- [33] X.B. Yuan, Y.H. Liu, B.X. Huang, C.J. Wang, L.M. Mei, *J. Phys D: Appl. Phys.* 38 (2005) 1.